Ultrasonics in an Aluminum Foam

Richard Weaver
Theoretical and Applied Mechanics
University of Illinois
104 South Wright Street
Urbana, IL 61801

Abstract:

Open celled foamed aluminum typically consists of an irregular frame of solid struts with typical lengths of the order of millimeters and thicknesses of a fraction of a millimeter. Total aluminum volume fractions are of the order of 10%. Quoted values of static modulus and mass density allow one to infer long wavelength (much greater than strut length) ultrasonic wave speeds. These predictions are compared with the velocities observed in 100kHz transient signals.

At higher frequencies, where wavelengths are comparable to strut lengths, ultrasound can be transported only diffusively. Wavespeeds are unmeasurable, and of little meaning anyway. We therefore also report on ultrasonic measurements appropriate for the high frequency regime. These include diffusivity, absorption and modal density. Recent literature has reported measurements of diffusivities and absorption in other materials, particularly in metallic polycrystals. Measurements of modal densities are new.

Ultrasonics in an Aluminum Foam

Richard Weaver
Theoretical and Applied Mechanics
University of Illinois
104 South Wright Street
Urbana, IL 61801

Introduction

Ultrasonic nondestructive characterization of materials with complex microstructures commonly proceeds by measurements of ultrasonic wave speed, attenuation, or backscatter. Wave speed measurement provides information on volume-averaged effective moduli and is relatively insensitive to details of microstructure. Attenuation, in many cases largely due to scattering from microstructural heterogeneities, provides a better probe of microstructural detail. Unambiguous measurements of attenuation are, however, sometimes difficult; and clear separation of the effects of diffraction and absorption from those of attenuation impossible.

Measurement of backscatter from the micro-heterogeneities, or "grain noise," is increasingly proposed as an alternative method for ultrasonic microstructure characterization. Amongst the difficulties in backscatter measurements, however, is the need to assume that the scattered signals represent rays that have scattered exactly once from the microstructure. Multiple scattering complicates the analysis.

These difficulties are most severe in materials with extremely strongly scattering microstructures. Scattering at long wavelengths is weakest, so it is often possible to confine one's ultrasonic tests to the lower frequencies and thereby avoid the difficulties discussed above. The shorter wavelengths, however, presumably carry more information on the details of the microstructure. It is therefore desirable to inquire as to whether short wavelength, high frequency, ultrasonics can be employed to ascertain material character.

The work reported here concerns the use of ultrasonics in the 200 kHz to 2 MHz range in an open-celled aluminum foam. The material is manufactured by ERG-Aerospace in Oakland California (web site: http://www.ergaerospace.com) and is available in a range of pore sizes (between five and 40 pores-per-inch) and porosities (typically 7%). A sample is shown in Figure[1]. The structure is nominally isotropic and consists of short struts of lengths of the order of one millimeter and widths of the order of one quarter the lengths, joined at three-strut junctions. Theoretical and experimental analyses of their static elastic and plastic properties do exist. See, for example, the paper on mechanics of cellular solids by Ashby[1].

The history of ultrasonics in this parameter regime is limited. Guo *et al*[2] studied multiply scattered diffuse ultrasound in polycrystalline iron. Weaver *et al*[3,4] did similar work on brasses and steels. Weaver and Sachse[5] studied diffuse multiply scattered ultrasound in a slurry of glass beads in water. The theory of such scattering is discussed by Weaver[6], and by Turner and Weaver[7] and by Ryzhik *et al.*[8] Throughout this literature it is concluded that the energy density (energy per frequency and per volume) of a multiply scattered diffuse ultrasonic field should evolve, at sufficiently late times after many scatterings, in accord with a diffusion equation. The laboratory work[2-5] in this regime has been largely confined to

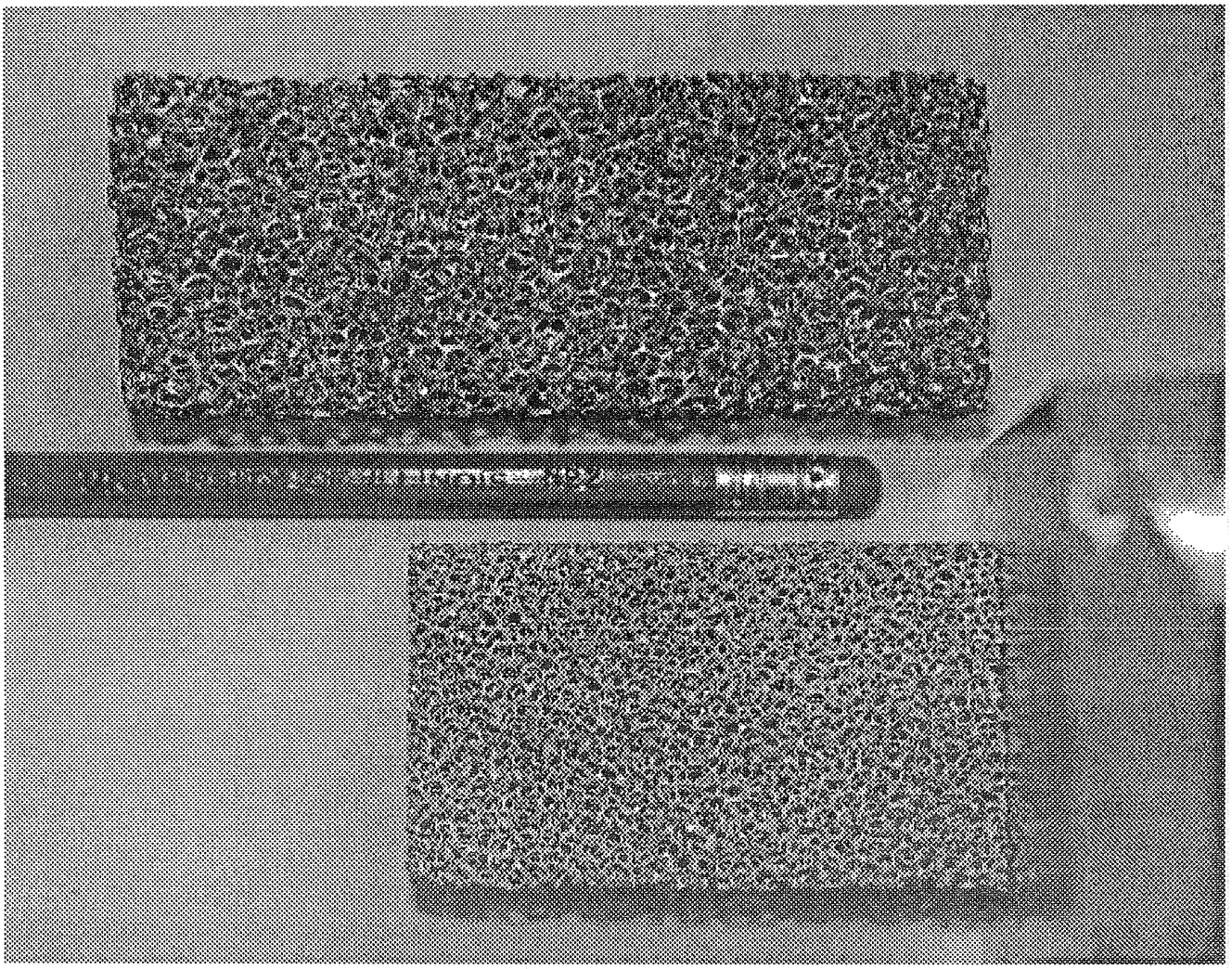

Figure 1] Photograph of the samples used in this study.

characterizing the phenomenological parameters of that diffusion equation - the diffusivity and the absorption. In this paper that procedure is followed once more, but the material is also characterized by means of measurement of its ultrasonic modal density (modes per volume per frequency.)

At long wavelengths, substantially greater than the strut lengths of ~1 mm, one could inquire as to the properties of air-borne acoustics through such foams. At frequencies less than ~50kHz, air-borne ultrasound may be imagined as propagating with little disturbance except for losses due to viscous and thermal processes at the abundant metal/air interface. The present paper is not concerned with air-borne ultrasound.

One could also, in an immersed sample of the foam, ask for the effective properties at frequencies substantially less than 250 kHz, at which wavelengths/2π are greater than strut lengths. A Biot-like mixture theory, with shear waves in the solid frame, and two different longitudinal waves, is likely to be applicable. This paper is not concerned with fluid saturated foams.

The ultrasound of interest here is borne by the solid frame, with little if any interaction with the air in which the sample is immersed. At sufficiently low frequency, where wavelengths/2π are greater than strut lengths, one anticipates an effective medium, with little attenuation, and wave speeds given by the square root of the ratio of the effective static moduli and the material density. According to the paper by Ashby[1], the static moduli are of the order of p^2 times those of the parent bulk aluminum, where p is the porosity (7% in the samples studied here). The density is p times the density of bulk aluminum. Thus one expects wave speeds at long wavelengths to be $\sqrt{p}$, or 26%, of those of bulk aluminum. The requirement that shear wavelengths / 2π = c_{shear} / ω be greater than strut lengths, then translates to a frequency regime f < 120kHz.

In the opposite limit, in which wavelengths are substantially less than strut lengths, one pictures ultrasound propagating along struts, at guided-mode speeds comparable to those of bulk aluminum, and scattering at the junctions. The picture is valid only if wavelengths are less than strut lengths, or f > 3 MHz. At intermediate frequencies one anticipates some kind of transition, as mean free paths vary between infinity at long wavelengths to 1 mm at short wavelengths, and as speeds vary between one quarter those of bulk aluminum at low frequencies to those of bulk aluminum at high frequencies. It is in this intermediate regime that the tests to be reported have been conducted.

Initial tests, in a conventional configuration, were conducted by pulse-echo contact ultrasonics using a 500kHz broad band piezoelectric transducer applied to one face of a 18 mm thick slab of the material. The transducer was coupled to the foam with water, and with grease. Even after repetition averaging, no back-wall reflected signal was detected. Indeed, no reflection was detected at all. The reason for the complete lack of echo is not certain. While one expects high attenuation at this frequency and a consequent weak back-wall reflection, one might have nevertheless expected some backscattered grain noise. The observed lack of grain noise suggests that the coupling was too weak. The transducer presumably coupled to the rough-surface foam at a small number of asperities, each of which was presumably highly compliant, with a consequent poor impedance match.

In a point/source point receiver configuration, using Valpey-Fisher pin-transducers with diameters of about 2 mm, one may apply the transducers to individual struts and junctions, and improve the coupling. A waveform from the configuration shown in Figure [2] is shown in Figure [3].

An expanded view of the early time part of this waveform is shown in figure 4]. It is

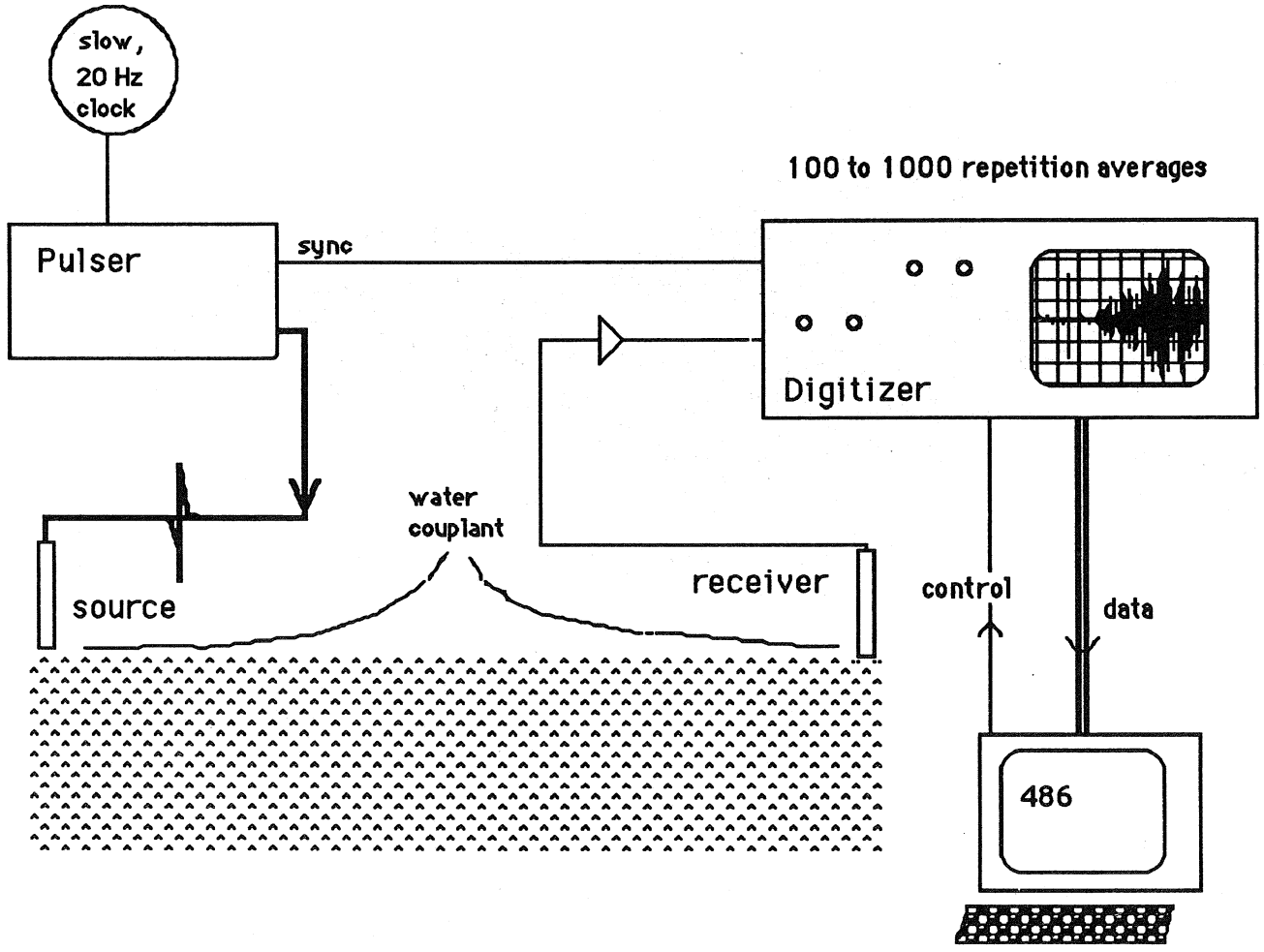

Figure 2] Point Source / Point Receiver Configuration

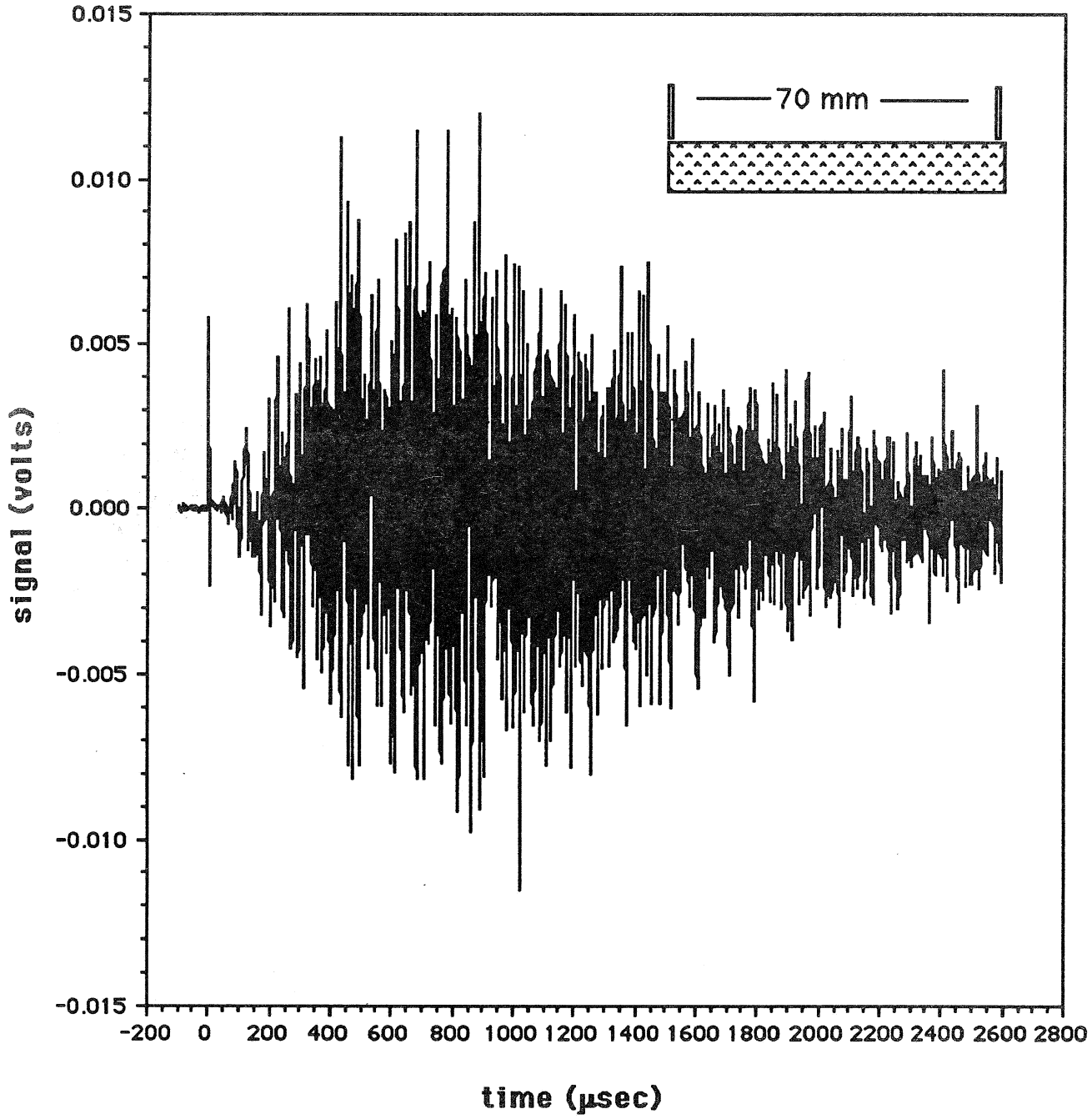

Figure 3] A point source/point receiver waveform obtained in the configuration shown, after 100 repetition averages.

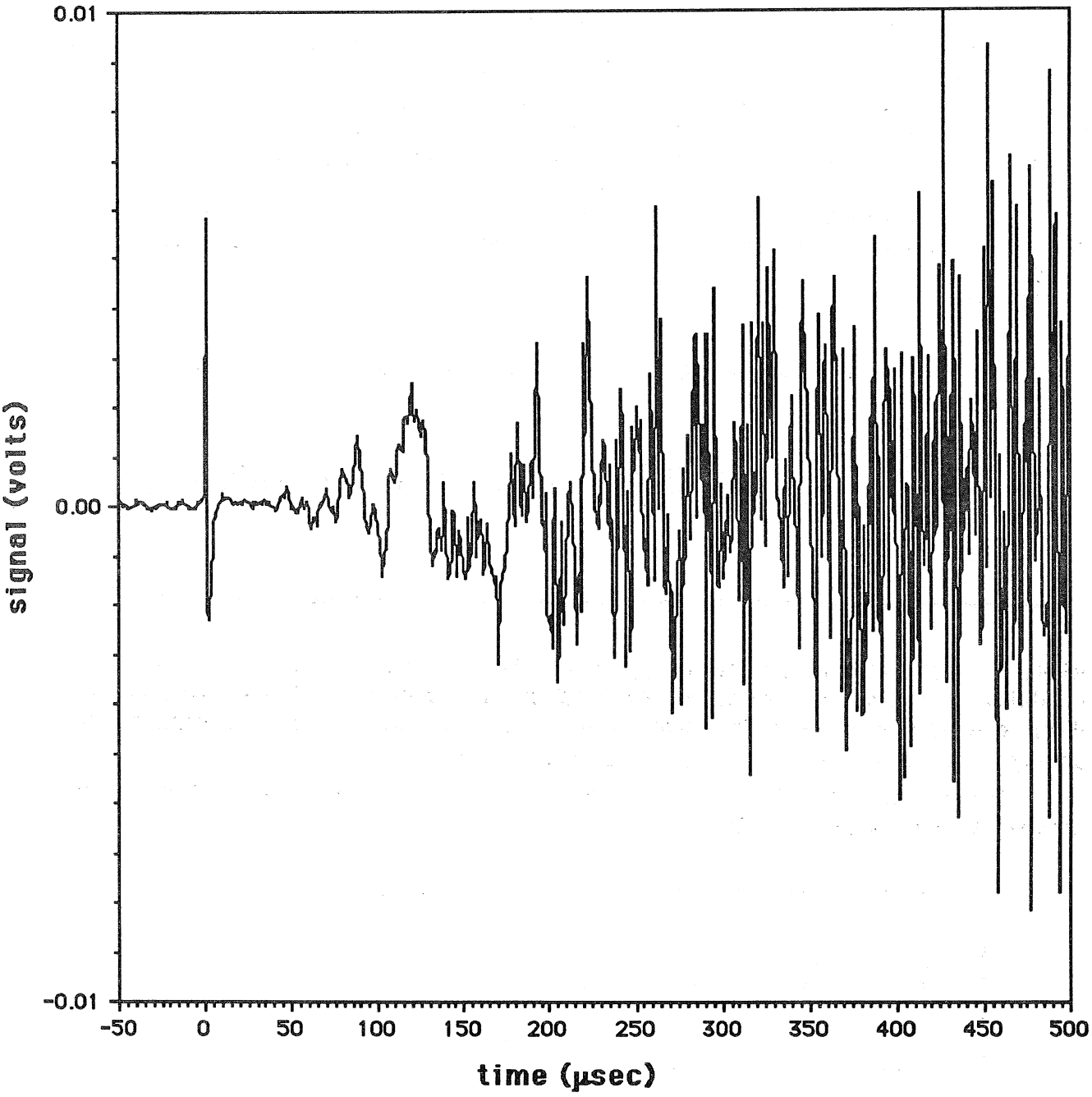

Figure 4] The waveform of figure 3 shown on an expanded time scale.

seen that there is an arrival at about 45 μsec, with a frequency of about 70 kHz . This corresponds to a low frequency wavespeed of 1.56 mm/ μsec, well in accord with the theoretical estimate of 26% of the bulk wave speed in aluminum. Wavespeeds obtained by similar scrutiny of other waveforms, from different source/receiver configurations, are also consistent with this estimate. In all cases, however, the first arrival has a frequency of the order or less than 100kHz. Higher frequencies are present in the waveform, but arrive more slowly. They are not as characterizable by means of an arrival time.

At higher frequencies one is led to attempt an analysis like that of Guo *et al*[2] or Weaver *et al*[3,4,5] in which the evolving energy density is fit to the solution of a modified diffusion equation.

$$\frac{\partial E(\vec{x},t)}{\partial t} = D \nabla^2 E(\vec{x},t) - \sigma E(\vec{x},t) + \Pi(\vec{x},t) \qquad (1$$

where E(x,t) is ultrasonic spectral energy density (energy per volume, per frequency bandwidth), and D is frequency-dependent diffusivity (with dimensions of length squared per time); σ is absorptivity (with dimensions of inverse time) and Π is the input spectral power density. Π is concentrated in space and time for a point impulsive source.

D is characteristic of the microstructure, and is nominally identifiable with the product of speed and mean free path L [6].

$$D = c L / 3 = c / 6 \alpha \qquad (2$$

This identification, however, requires that one be able to unambiguously quantify c and L. The phenomenological quantity D, however, presumably has legitimacy in conditions in which c and L may be ambiguous.

The absorptivity σ is due to (linear) loss mechanisms, for example internal friction, dislocation motion, or loss into an adjacent fluid.

As described elsewhere[2-5], waveforms such as that of figure 3 may be analyzed for their fit to solutions of equation(1) by first doing a time-frequency analysis. The waveform is arbitrarily divided into time windows (in this case of width Δt =102 μsec each) and each time window is given smoothed edges and separately Fourier analyzed. For each time-window the resulting spectrum is then squared and integrated over a frequency bin of arbitrary width Δf (in this case equal to 156 kHz). The result is a table of power spectral densities E(f,t) at each of several times and in each of several frequency bins. The resulting quantity E is not precisely ultrasonic spectral energy density itself (in ergs per cm^3 per kHz) but differs from that by a factor related to transducer sensitivity and a factor relating the measured local mean square motions detected by the transducer to the local strain and kinetic energy densities. That factor is unknown, but presumed constant.

It also differs in that the waveform is stochastic, and so E, as constructed by the above procedure, is only statistically representative of the actual local energy density. One could cope with the resulting uncertainty by averaging, over a small region in space, or over an ensemble of equivalent samples, but that is not necessary.

Assuming Gaussian statistics (based on an application of the central limit theorem and assuming a large number of contributing rays at any given place and time), and assuming near stationarity (across each frequency bin and across each time window) one can show that the measured energy density fluctuates away from its ensemble average by one part in the square root of the product of Δt and Δf.

$$E = E_{measured} \pm \{ 1 / \sqrt{\Delta t \, \Delta f} \} \; E_{measured} \qquad (3$$

In the present tests this is, for Δf = 156 kHz; Δt = 102 μsec,

$$\pm 1 / \sqrt{\Delta t \, \Delta f} = \pm 25\%. \qquad (4$$

But, the effective value of Δf may be much less than the nominal 156 kHz. Fourier Transforms of the full waveform show a very irregular spectrum, and stationarity in frequency is not well satisfied.

The fluctuations are reducible by increasing Δt and/or Δf - with consequent loss of time or frequency resolution. The fluctuations are in principle also reducible by spatial averaging over small regions.

A typical plot of the logarithms of the tabulated energies, versus time for each of several frequency bins, is shown in figure[5]. It may be noted that a) there is an electronic noise level substantially less than signal level; b) there is cross talk from source to receiver circuits at the trigger time; c) the energy arrives over a distance of 70 mm on a time scale of nearly a msec, corresponding to diffusive transport and not propagation; d) the late time behavior is dominated by absorption with different frequency bins having different absorptivities; and e) there are occasional excess fluctuations in bins and times at which the fluctuations exceed ±25%, but that generally fluctuations lie within the stated error bars.

Fit procedure:

The solution to the lossy diffusion equation (1) in an infinite one-dimensional medium is

$$E(x,t) = \frac{\text{Constant}}{\sqrt{Dt}} \exp\{ -x^2/4Dt \} \exp\{ -\sigma t \} \qquad (5$$

where the constant depends on the amount of deposited energy. In a one-dimensional bar of finite length this solution must be supplemented by additional terms, of similar form, due to image sources. If the source and receiver are at opposite ends of the finite bar there is one image source adjacent to the actual source, and two on the opposite side; all three are at the same distance from the receiver as the real source; their effect is merely to quadruple the above expression. The next closest image source is at a distance of three bar-lengths from the receiver; it therefore does not contribute significantly until very late times ($t > 9 * \text{length}^2 / 4D$), times which we later find (after evaluating D) to be outside the range examined here.

In a bar of finite cross section, there are also effects, at early times, due to the finite rate at which the diffusing energy field establishes an equilibrium distribution across the bar thickness. As the source and receiver were placed at the midpoints of their respective ends, this takes place on a time scale $t \sim \text{width}^2/4\pi^2 D$. The two transverse dimensions were 18 and 38 mm, which correspond to time scales far shorter than all of the time scales examined in this work.

In consequence of the relative dimension of the bars used, and the time scales examined, and the actual rate of diffusion, the energy evolves as if it were in an infinite thin bar. Its logarithm evolves according to

$$\log_e E(t) = A - \sigma t - x^2 / 4 D t - (1/2) \log_e t \qquad (6$$

where x = 70 mm is the bar length.

This expression is a linear functional of three unknown coefficients, A (related to amount of energy deposited), σ, which is interpreted as absorptivity, and $x^2/4D$, related to the diffusivity. For each frequency band, and for the time range in which the signal is clearly above the noise, the observed $\log_e E$'s are then fit by simple *linear regression* to these three parameters.

In more complex geometries, where the bar is not modelable as infinitely long and infinitely narrow, one would need to do a *non-linear regression*, and the fit procedure would be more cumbersome. This is discussed in references[3,4].

The fit parameters extracted from the linear regression are plotted in figure [6] versus frequency.

As is usually the case, the absorptivity rises with frequency, approximately linearly. The physical mechanisms behind the absorption are not clear. The recovered values exceed the values one would estimate for losses into air . They furthermore have been found to decrease on chemical polishing, and to increase with exposure to oils. It is surmised that most of the absorption is due to surface processes.

In a configuration in which both source and receiver are on the same end of the bar, the relevant solution to the diffusion equation is identical to (5)- except that x is set to zero. A two-parameter fit then allows recovery of absorptivity alone. If our sample has spatially

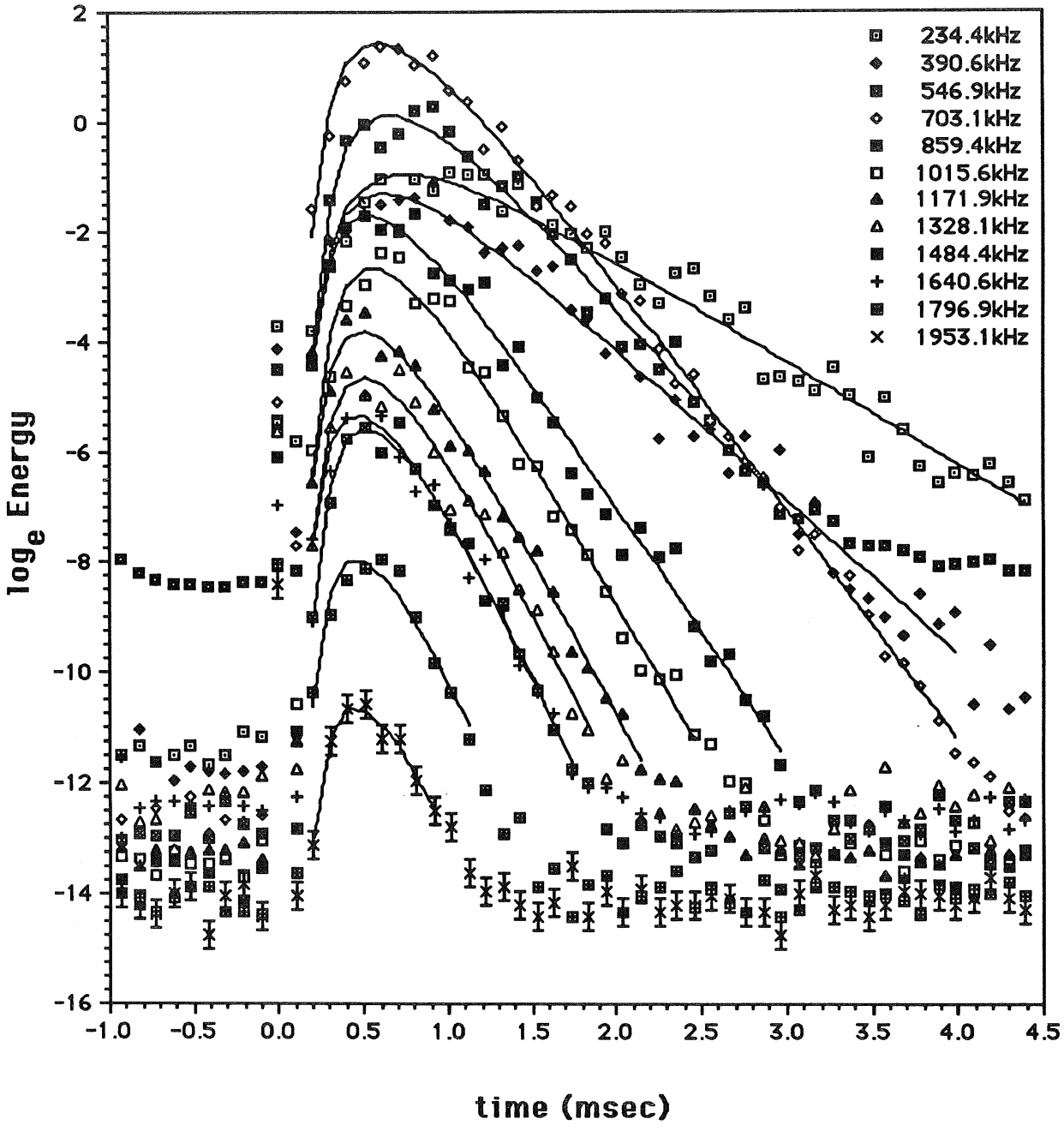

Figure 5] The observed ln E's are plotted versus time, and the best-fit solution to the diffusion equation superposed. Error bars are shown on one of the bins, but are the same for all.

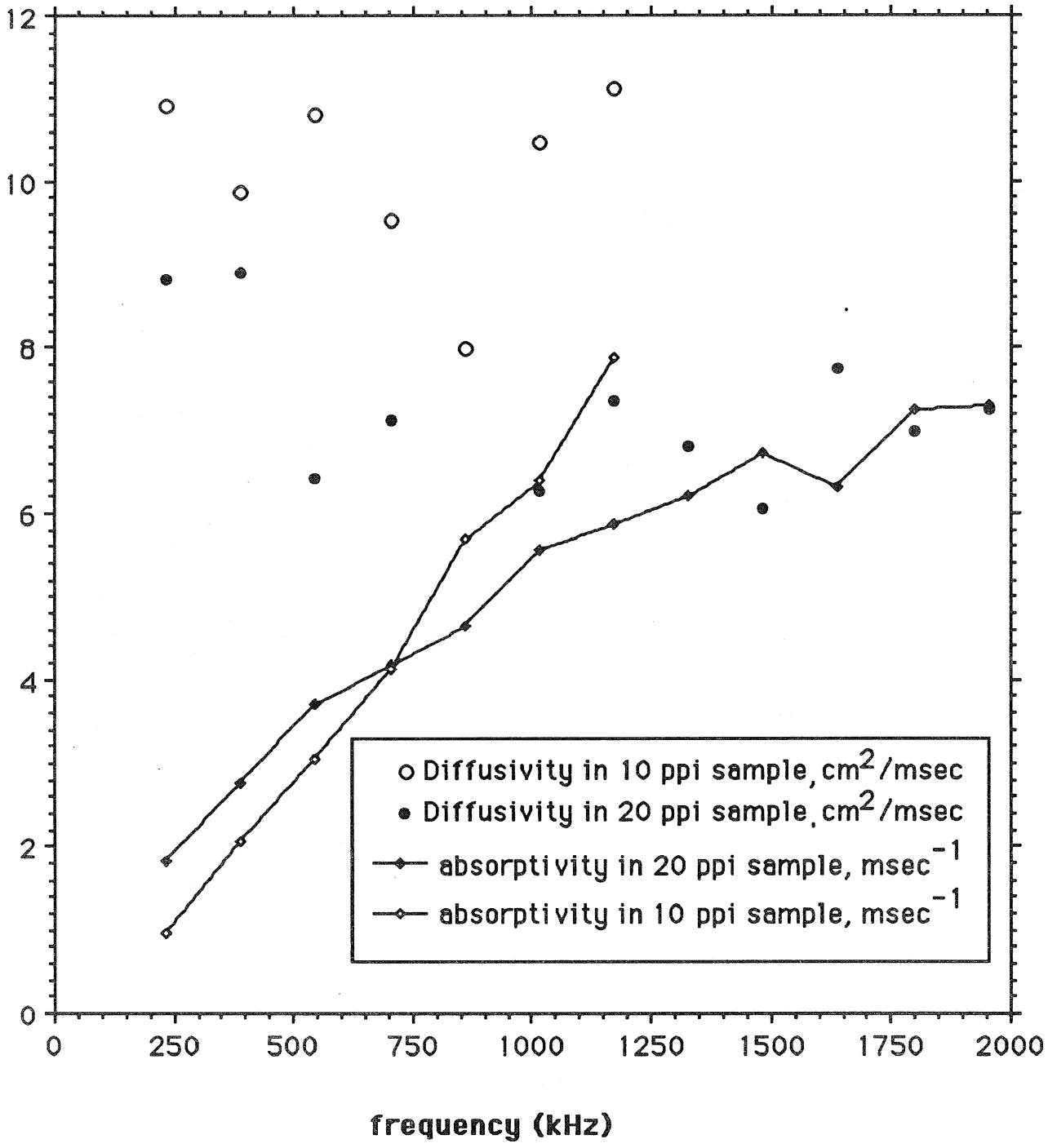

Figure 6] Recovered fit parameters from each of two samples of aluminum foam, the 10 pore-per inch and 20 pore per inch.

uniform absorptivity, and if the diffusion model is robust, the recovered absorptivity should be the same. The recovered absorptivities were found to be about 10% less in the new configuration, an amount judged, for now, to be negligible.

Similar tests have also been carried out in a 97 mm long bar of a 10 pore-per-inch material. The resulting fit parameters are also shown in figure 6.

Theory for diffusivity.

If the diffusion rate is a function of the elastic properties and of the microstructural geometry, then dimensional analysis says that D should be given by the following form

$$D = (1/3) * "c" * "L" * g(\omega L/c, \nu) \qquad (7$$

where "c" is a material wave speed, of the order of 3 mm/ μsec, ν is the micro-scale material Poisson ratio, g is a dimensionless function and "L" is the micro-scale length. The factor 1/3 is inserted in order to accentuate the similarity to equation(2).

If g is taken to be unity one concludes that D should be about 10 cm^2 / msec, by taking L = strut length =1 mm. This estimate is in accord with observations.

The theory also suggests that two samples, with different strut lengths, but otherwise exact scale versions of each other, will differ in their D's by a factor of the length scale ratio if one also keeps the product of frequency and L constant. Thus one would predict that the 20 ppi sample, at frequency f should have half the diffusivity of the 10 ppi sample at frequency f/2. This scaling is not precisely followed. For example, the diffusivity of the 10 ppi sample at 500 kHz is only 50% greater than that of the 20 ppi sample at 1 MHz. One surmises that the samples are not scale models of each other.

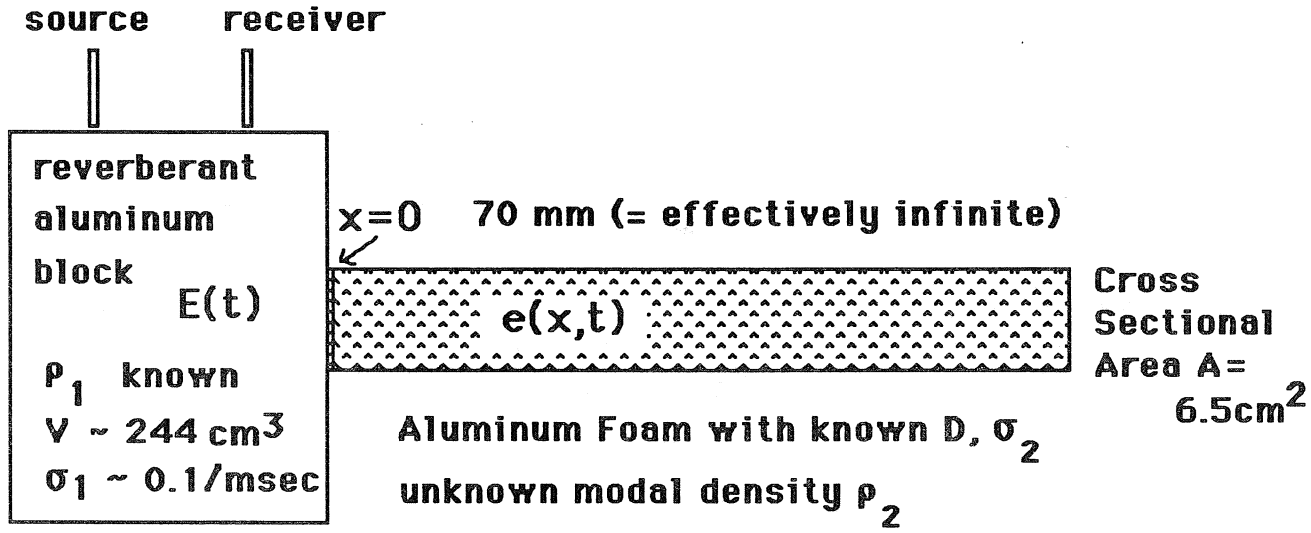

Figure 7] Composite sample used for evaluation of modal density.

Measurement of Modal Density

Two reverberant materials (with sufficiently good coupling between them) will, according to Statistical Energy Analysis[see e.g. 9], exchange ultrasonic energy until they achieve a steady-state dynamic balance with equal amounts of energy per normal-mode-of-vibration. This behavior may be used to evaluate the ratio of modal densities of two materials.

Here we conduct energy flow measurements on a composite structure composed of a solid aluminum block, with known modal density (known from theory), and known absorptivity (determined from prior measurements) which is coupled (by means of superglue) to the end of the 20 ppi sample of aluminum foam. The configuration is indicated in figure (7).

Energy flow equations for this system, the generalization of (1), are,

$$\frac{\partial}{\partial t} E(t) = -\sigma_1 E(t) - F(t) + \delta(t)$$

$$\frac{\partial}{\partial t} e(x,t) = -\sigma_2 e(x,t) + D\, \partial^2 e(x,t) / \partial x^2 \qquad (8$$

$$F = \eta \{ E(t)/\rho_1 V - e(x,t)|_{x=0} / \rho_2 A \}$$

$$F = -D\, \partial e(x,t) / \partial x |_{x=0}$$

where F represents the power flow from the block into the foam. F is proportional (with coefficient η) to the difference of energy per mode in the two materials at the contact point. The diffusion equation in the foam is supplemented by a boundary condition on the power flow at the contact point.

We assume i) Good Coupling, i.e. large η, between materials and ii) no added losses due to glue, and solve these energy flow equations using Laplace Transforms. It is concluded that the asymptotic behavior of the energy in the block is an exponential decay like

$$E_1 \sim \exp\{ - \sigma_{effective}\ t\} \qquad (9$$

where the effective, late time, absorptivity of the composite is given by

$$\sigma_{effective} = \sigma_1 + (\sigma_2 - \sigma_1)\frac{P}{2}[\sqrt{1+4/P} - 1] \qquad (10$$

$$\text{where } P \equiv D\left(\frac{A}{V}\right)^2\left(\frac{\rho_{Duocel}}{\rho_{aluminum\ Block}}\right)^2 / (\sigma_2 - \sigma_1)$$

$\sigma_{effective}$ is a weighted average of the absorptions in each material, weighted by an amount that depends on the penetration depth of the field into the foam. This behavior is only asymptotic; there is a, possibly short, initial time period over which the block and foam come into a steady state dynamic balance.

By measurement of $\sigma_{effective}$ (the slope of the asymptotic decay) and by knowing D and σ_1 and σ_2, one can construct the ratio of the modal densities of the Foam and the reference Block. This has been done for each of two configurations of source and receiver: one with both on the block, one with both on the foam, but adjacent to the block. The resulting asymptotic decay rates were the same. A plot of the resulting energy density evolution is shown in figure (8). It may be seen that the early time behavior is more complex than the late time simple asymptotic exponential decay.

The recovered ratio of the modal density of the foam to that of the aluminum block is shown in figure (9). One may also construct theoretical estimates of the low frequency and high frequency limits. At low frequency one may invoke an effective medium argument and recognize that model densities scale inversely with the third power of wave speed, and so the low frequency ratio should be $(.26)^{-3} = 57$. At very high frequency, with wavelengths less than strut widths, one can picture bulk waves in aluminum propagating within the struts and derive a modal density which is p = 7% of that of bulk aluminum. The measured values lie, as one would hope, between these limits. The measured values show the expected decrease with increasing frequency, but not with the slope that one might have guessed.

Conclusions:

Conventional Ultrasonic Methods are inapplicable to materials with very strongly scattering, disordered, microstructures. But one can assess diffusivities, absorptivities, and modal densities. All values recovered in the samples studied appear plausible, and are consistent with the rather limited theoretical understanding. The recovered values, and the applicability of the diffuse field theory and assumptions behind them, need to be further corroborated by further measurements.

Acknowledgement

This work has been supported by the National Science Foundation through grant number CMS-9701142. Samples provided by ERG-Aerospace are also gratefully acknowledged.

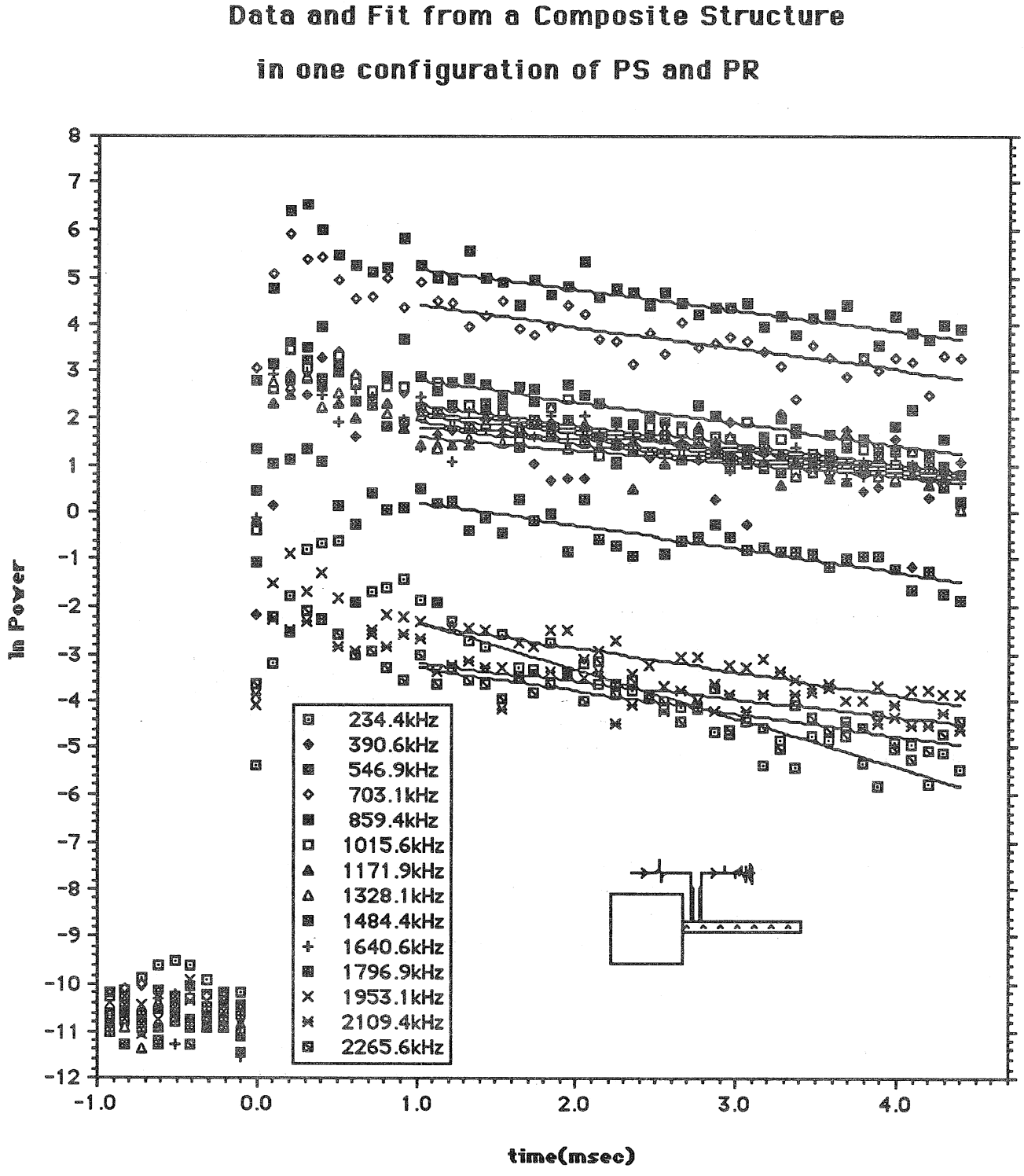

Figure 8] Energy Evolution in the composite sample, and its superposed fit to an asymptotic exponential decay.

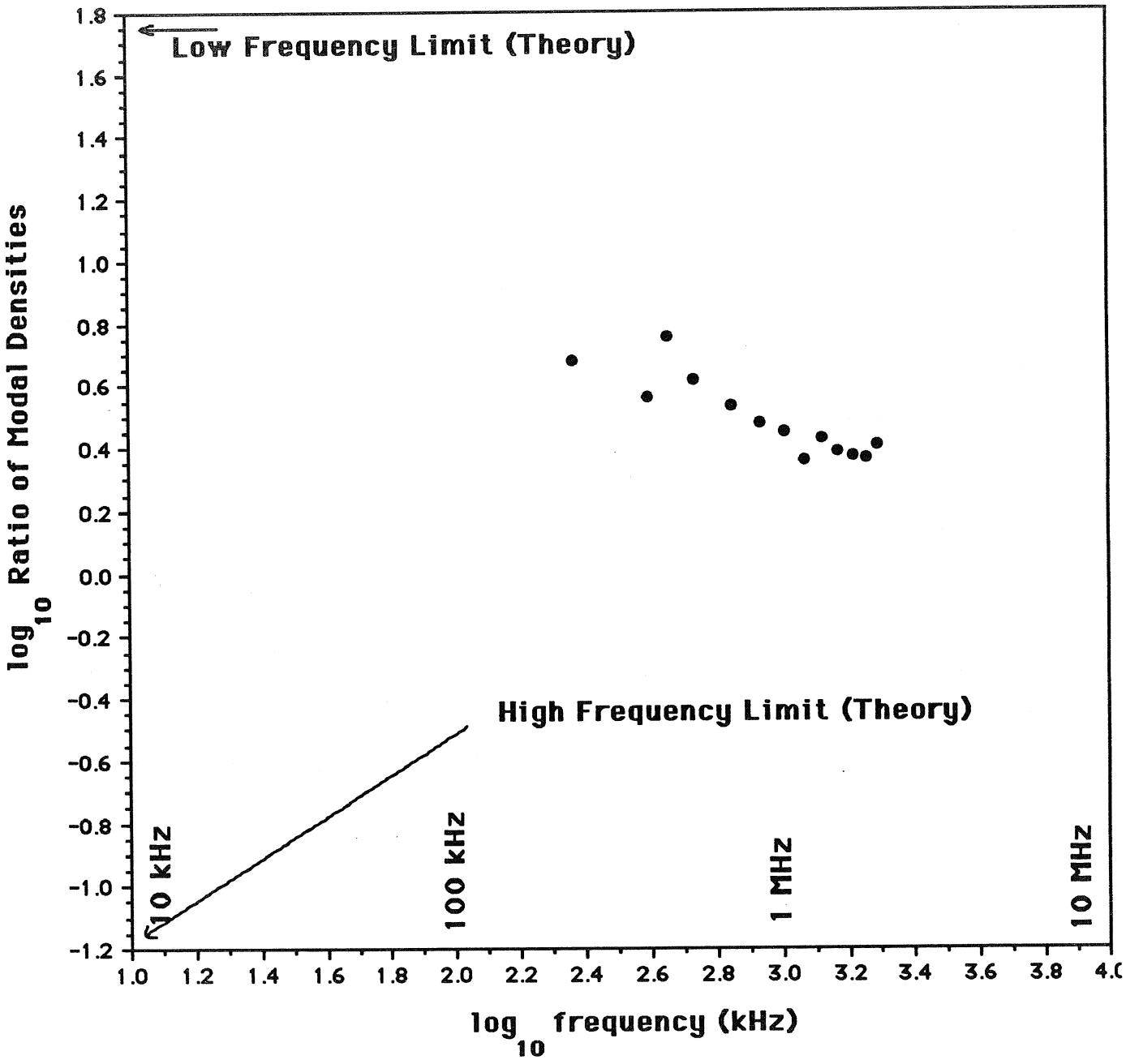

Figure 9] The recovered values of the ratio of modal density in the foam sample and in bulk aluminum, plotted *versus* frequency.

References

1] M F Ashby, "The Mechanical properties of cellular solids," *Metal Trans A* 14, 1755-1769 (1983)

2] C. B. Guo, P Holler and K Goebbels, "Scattering of UT waves in anisotropic polycrystalline Metals," *Acustica* 59, 112-120 (1985)

3] R. Weaver, W. Sachse, K. Green, and Y. Zhang, "Diffuse ultrasound in polycrystalline solids," Proceedings of Ultrasonics International91,p 507-510, Butterworth-Heinemann (1991)

4] R. Weaver, "Ultrasonic Diffuse Field Measurements of Grain Size," in Non-Destructive Testing and Evaluation in Manufacturing and Construction, Henrique L. M. dos Reis, ed. Hemisphere p425-434, (1990).

5] R.L. Weaver and W. Sachse, "Diffusion of ultrasound in a glass bead slurry," *J. Acoust. Soc. Am.* **97**, 2094-2102 (1995)

6] R. Weaver, "Diffusivity of Ultrasound in Polycrystals," *J. Mechs. and Phys. of Solids.* 38, 55-86 (1990).

7] J. A. Turner and R.L. Weaver, "Radiative Transfer of Ultrasound: Effects of a solid/fluid interface," *J.Acoust.Soc.Am.* **98**, *2801-2808* (1995)

8] L. V. Ryzhik, G. Papanicolaou, and J. B. Keller, "Transport equations for elastic and other waves in random media," *Wave Motion* 24, p 327-370 (1997)

9] R.L. Weaver, "Diffuse Waves on Submerged Thin Shells," *J.Acoust.Soc.Am.* **95**, 857-865 (1994)

List of Recent TAM Reports

No.	Authors	Title	Date
772	Aref, H., and S. W. Jones	Motion of a solid body through ideal fluid—Proceedings of the DCAMM 25th Anniversary Volume, 55–68 (1994)	Oct. 1994
773	Stewart, D. S., T. D. Aslam, J. Yao, and J. B. Bdzil	Level-set techniques applied to unsteady detonation propagation—In "Modeling in Combustion Science," *Lecture Notes in Physics* , eds. J. Buckmaster and J. Takeno **126**, 390–409 (1996)	Oct. 1994
774	Mittal, R., and S. Balachandar	Effect of three-dimensionality on the lift and drag of circular and elliptic cylinders—*Physics of Fluids* **7**, 1841–1865 (1995)	Oct. 1994
775	Stewart, D. S., T. D. Aslam, and J. Yao	On the evolution of cellular detonation	Nov. 1994 *Revised* Jan. 1996
776	Aref, H.	On the equilibrium and stability of a row of point vortices—*Journal of Fluid Mechanics* **290**, 167–181 (1995)	Nov. 1994
777	Cherukuri, H. P., T. G. Shawki, and M. El-Raheb	An accurate finite-difference scheme for elastic wave propagation in a circular disk—*Journal of the Acoustical Society of America*, in press (1996)	Nov. 1994
778	Li, L., and N. R. Sottos	Improving hydrostatic performance of 1–3 piezocomposites—*Journal of Applied Physics* **77**, 4595–4603 (1995)	Dec. 1994
779	Phillips, J. W., D. L. de Camara, M. D. Lockwood, and W. C. C. Grebner	Strength of silicone breast implants—*Plastic and Reconstructive Surgery* **97**, 1215–1225 (1996)	Jan. 1995
780	Xin, Y.-B., K. J. Hsia, and D. A. Lange	Quantitative characterization of the fracture surface of silicon single crystals by confocal microscopy—*Journal of the American Ceramics Society* **78**, 3201–3208 (1995)	Jan. 1995
781	Yao, J., and D. S. Stewart	On the dynamics of multi-dimensional detonation—*Journal of Fluid Mechanics* **309**, 225–275 (1996)	Jan. 1995
782	Riahi, D. N., and T. L. Sayre	Effect of rotation on the structure of a convecting mushy layer—*Acta Mechanica* **118**, 109–120 (1996)	Feb. 1995
783	Batchelor, G. K., and TAM faculty and students	A conversation with Professor George K. Batchelor	Feb. 1995
784	Sayre, T. L., and D. N. Riahi	Effect of rotation on flow instabilities during solidification of a binary alloy—*International Journal of Engineering Science* **34**, 1631–1645 (1996)	Feb. 1995
785	Xin, Y.-B., and K. J. Hsia	A technique to generate straight surface cracks for studying the dislocation nucleation condition in brittle materials—*Acta Metallurgica et Materialia* **44**, 845–853 (1996)	Mar. 1995
786	Riahi, D. N.	Finite bandwidth, long wavelength convection with boundary imperfections: Near-resonant wavelength excitation—*International Journal of Mathematics and Mathematical Sciences*, in press (1996)	Mar. 1995
787	Turner, J. A., and R. L. Weaver	Average response of an infinite plate on a random foundation—*Journal of the Acoustical Society of America* **99**, 2167–2175 (1996)	Mar. 1995
788	Weaver, R. L., and D. Sornette	The range of spectral correlations in pseudointegrable systems: GOE statistics in a rectangular membrane with a point scatterer—*Physical Review E* **52**, 341 (1995)	Apr. 1995
789	Students in TAM 293–294	Thirty-second student symposium on engineering mechanics, J. W. Phillips, coordinator: Selected senior projects by K. F. Anderson, M. B. Bishop, B. C. Case, S. R. McFarlin, J. M. Nowakowski, D. W. Peterson, C. V. Robertson, and C. E. Tsoukatos	Apr. 1995
790	Figa, J., and C. J. Lawrence	Linear stability analysis of a gravity-driven Newtonian coating flow on a planar incline	May 1995
791	Figa, J., and C. J. Lawrence	Linear stability analysis of a gravity-driven viscosity-stratified Newtonian coating flow on a planar incline	May 1995

List of Recent TAM Reports (cont'd)

No.	Authors	Title	Date
792	Cherukuri, H. P., and T. G. Shawki	On shear band nucleation and the finite propagation speed of thermal disturbances—*International Journal of Solids and Structures,* in press (1996)	May 1995
793	Harris, J. G.	Modeling scanned acoustic imaging of defects at solid interfaces—Chapter in *IMA Workshop on Inverse Problems in Wave Propagation,* eds. G. Chevant, G. Papanicolaou, P. Sacks and W. E. Symes, 237–258, Springer-Verlag, New York (1996)	May 1995
794	Sottos, N. R., J. M. Ockers, and M. J. Swindeman	Thermoelastic properties of plain weave composites for multilayer circuit board applications	May 1995
795	Aref, H., and M. A. Stremler	On the motion of three point vortices in a periodic strip—*Journal of Fluid Mechanics* **314**, 1–25 (1996)	June 1995
796	Barenblatt, G. I., and N. Goldenfeld	Does fully-developed turbulence exist? Reynolds number independence versus asymptotic covariance—*Physics of Fluids* **7**, 3078–3082 (1995)	June 1995
797	Aslam, T. D., J. B. Bdzil, and D. S. Stewart	Level set methods applied to modeling detonation shock dynamics—*Journal of Computational Physics,* **126**, 390–409 (1996)	June 1995
798	Nimmagadda, P. B. R., and P. Sofronis	The effect of interface slip and diffusion on the creep strength of fiber and particulate composite materials—Proceedings of the ASME Applied Mechanics Division **213**, 125–143 (1995)	July 1995
799	Hsia, K. J., T.-L. Zhang, and D. F. Socie	Effect of crack surface morphology on the fracture behavior under mixed mode loading—*ASTM Special Technical Publication* 1296, in press (1996)	July 1995
800	Adrian, R. J.	Stochastic estimation of the structure of turbulent fields—*Eddy Structure Identification,* ed. J. P. Bonnet, Springer: Berlin 145–196 (1996)	Aug. 1995
801	Riahi, D. N.	Perturbation analysis and modeling for stratified turbulence	Aug. 1995
802	Thoroddsen, S. T.	Conditional sampling of dissipation in high Reynolds number turbulence—*Physics of Fluids* **8**, 1333–1335	Aug. 1995
803	Riahi, D. N.	On the structure of an unsteady convecting mushy layer—*Acta Mechanica,* in press (1996)	Aug. 1995
804	Meleshko, V. V.	Equilibrium of an elastic rectangle: The Mathieu–Inglis–Pickett solution revisited—*Journal of Elasticity* **40**, 207–238 (1995)	Aug. 1995
805	Jonnalagadda, K., G. E. Kline, and N. R. Sottos	Local displacements and load transfer in shape memory alloy composites	Aug. 1995
806	Nimmagadda, P. B. R., and P. Sofronis	On the calculation of the matrix–reinforcement interface diffusion coefficient in composite materials at high temperatures—*Acta Metallurgica et Materialia,* **44**, 2711–2716 (1996)	Aug. 1995
807	Carlson, D. E., and D. A. Tortorelli	On hyperelasticity with internal constraints—*Journal of Elasticity* **42**, 91–98 (1966)	Aug. 1995
808	Sayre, T. L., and D. N. Riahi	Oscillatory instabilities of the liquid and mushy layers during solidification of alloys under rotational constraint—*Acta Mechanica* **121** , 143–152 (1997)	Sept. 1995
809	Xin, Y.-B., and K. J. Hsia	Simulation of the brittle–ductile transition in silicon single crystals using dislocation mechanics	Oct. 1995
810	Ulysse, P., and R. E. Johnson	A plane-strain upper-bound analysis of unsymmetrical single-hole and multi-hole extrusion processes	Oct. 1995
811	Fried, E.	Continua described by a microstructural field—*Zeitschrift für angewandte Mathematik und Physik,* **47**, 168–175 (1996)	Nov. 1995
812	Mittal, R., and S. Balachandar	Autogeneration of three-dimensional vortical structures in the near wake of a circular cylinder	Nov. 1995
813	Segev, R., E. Fried, and G. de Botton	Force theory for multiphase bodies—*Journal of Geometry and Physics,* in press (1996)	Dec. 1995

List of Recent TAM Reports (cont'd)

No.	*Authors*	*Title*	*Date*
814	Weaver, R. L.	The effect of an undamped finite-degree-of-freedom "fuzzy" substructure: Numerical solutions and theoretical discussion—*Journal of the Acoustical Society of America* **100**, 3159–3164 (1996)	Jan. 1996
815	Haber, R. B., C. S. Jog, and M. P. Bendsøe	A new approach to variable-topology shape design using a constraint on perimeter—*Structural Optimization* **11**, 1–12 (1996)	Feb. 1996
816	Xu, Z.-Q., and K. J. Hsia	A numerical solution of a surface crack under cyclic hydraulic pressure loading	Mar. 1996
817	Adrian, R. J.	Bibliography of particle velocimetry using imaging methods: 1917–1995—*Produced and distributed in cooperation with TSI, Inc., St. Paul, Minn.*	Mar. 1996
818	Fried, E., and G. Grach	An order-parameter based theory as a regularization of a sharp-interface theory for solid–solid phase transitions—*Archive for Rational Mechanics and Analysis,* in press (1996)	Mar. 1996
819	Vonderwell, M. P., and D. N. Riahi	Resonant instability mode triads in the compressible boundary-layer flow over a swept wing—*Physics of Fluids*, in press (1996)	Mar. 1996
820	Short, M., and D. S. Stewart	Low-frequency two-dimensional linear instability of plane detonation—*Journal of Fluid Mechanics*, in press (1997)	Mar. 1996
821	Casagranda, A., and P. Sofronis	On the scaling laws for the consolidation of nanocrystalline powder compacts—Proceedings of the IUTAM Symposium on the Mechanics of Granular and Porous Materials (1996)	Apr. 1996
822	Xu, S., and D. S. Stewart	Deflagration-to-detonation transition in porous energetic materials: A comparative model study—*Journal of Fluid Mechanics*, in press (1997)	Apr. 1996
823	Weaver, R. L.	Mean and mean-square responses of a prototypical master/fuzzy structure—*Journal of the Acoustical Society of America,* in press (1996)	Apr. 1996
824	Fried, E.	Correspondence between a phase-field theory and a sharp-interface theory for crystal growth—*Continuum Mechanics and Thermodynamics*, in press (1997)	Apr. 1996
825	Students in TAM 293–294	Thirty-third student symposium on engineering mechanics, J. W. Phillips, coordinator: Selected senior projects by W. J. Fortino II, A. A. Mordock, and M. R. Sawicki	May 1995
826	Riahi, D. N.	Effects of roughness on nonlinear stationary vortices in rotating disk flows—*Mathematical and Computer Modeling,* in press (1996)	June 1996
827	Riahi, D. N.	Nonlinear instabilities of shear flows over rough walls	June 1996
828	Weaver, R. L.	Multiple scattering theory for a plate with sprung masses: Mean and mean-square responses	July 1996
829	Moser, R. D., M. M. Rogers, and D. W. Ewing	Self-similarity of time-evolving plane wakes	July 1996
830	Lufrano, J. M., and P. Sofronis	Enhanced hydrogen concentrations ahead of rounded notches and cracks—Competition between plastic strain and hydrostatic constraint	July 1996
831	Riahi, D. N.	Effects of surface corrugation on primary instability modes in wall-bounded shear flows	Aug. 1996
832	Bechel, V. T., and N. R. Sottos	Measuring debond length in the fiber pushout test—Proceedings of the ASME Mechanics and Materials Conference (1996)	Aug. 1996
833	Riahi, D. N.	Effect of centrifugal and Coriolis forces on chimney convection during alloy solidification—*Journal of Crystal Growth,* in press (1997)	Sept. 1996
834	Cermelli, P., and E. Fried	The influence of inertia on configurational forces in a deformable solid—*Proceedings of the Royal Society of London A,* in press (1996)	Oct. 1996
835	Riahi, D. N.	On the stability of shear flows with combined temporal and spatial imperfections	Oct. 1996
836	Carranza, F. L., B. Fang, and R. B. Haber	An adaptive space–time finite element model for oxidation-driven fracture	Nov. 1996

List of Recent TAM Reports (cont'd)

No.	Authors	Title	Date
837	Carranza, F. L., B. Fang, and R. B. Haber	A moving cohesive interface model for fracture in creeping materials	Nov. 1996
838	Balachandar, S., R. Mittal, and F. M. Najjar	Properties of the mean wake recirculation region in two-dimensional bluff body wakes	Dec. 1996
839	Ti, B. W., W. D. O'Brien, Jr., and J. G. Harris	Measurements of coupled Rayleigh wave propagation in an elastic plate	Dec. 1996
840	Phillips, W. R. C.	On finite-amplitude rotational waves in viscous shear flows	Jan. 1997
841	Riahi, D. N.	Direct resonance analysis and modeling for a turbulent boundary layer over a corrugated surface	Jan. 1997
842	Liu, Z.-C., R. J. Adrian, C. D. Meinhart, and W. Lai	Structure of a turbulent boundary layer using a stereoscopic, large format video-PIV	Jan. 1997
843	Fang, B., F. L. Carranza, and R. B. Haber	An adaptive discontinuous Galerkin methods for viscoplastic analysis	Jan. 1997
844	Xu, S., T. D. Aslam, and D. S. Stewart	High-resolution numerical simulation of ideal and non-ideal compressible reacting flows with embedded internal boundaries	Jan. 1997
845	Zhou, J., C. D. Meinhart, S. Balachandar, and R. J. Adrian	Formation of coherent hairpin packets in wall turbulence	Feb. 1997
846	Lufrano, J. M., P. Sofronis, and H. K. Birnbaum	Elastoplastically accommodated hydride formation and embrittlement	Feb. 1997
847	Keane, R. D., N. Fujisawa, and R. J. Adrian	Unsteady non-penetrative thermal convection from non-uniform surfaces	Feb. 1997
848	Aref, H., and M. Brøns	On stagnation points and streamline topology in vortex flows	Mar. 1997
849	Asghar, S., T. Hayat, and J. G. Harris	Diffraction by a slit in an infinite porous barrier	Mar. 1997
850	Shawki, T. G., H. Aref, and J. W. Phillips	Mechanics on the Web—Proceedings of the International Conference on Engineering Education (Aug. 1997, Chicago)	Apr. 1997
851	Stewart, D. S., and J. Yao	The normal detonation shock velocity–curvature relationship for materials with non-ideal equation of state and multiple turning points	Apr. 1997
852	Fried, E., A. Q. Shen, and S. T. Thoroddsen	Traveling waves, standing waves, and cellular patterns in a steadily forced granular medium	Apr. 1997
853	Boyland, P. L., H. Aref, and M. A. Stremler	Topological fluid mechanics of stirring	Apr. 1997
854	Parker, S. J., and S. Balachandar	Viscous and inviscid instabilities of flow along a streamwise corner	May 1997
855	Soloff, S. M., R. J. Adrian, and Z.-C. Liu	Distortion compensation for generalized stereoscopic particle image velocimetry	May 1997
856	Zhou, Z., R. J. Adrian, S. Balachandar, and T. M. Kendall	Mechanisms for generating coherent packets of hairpin vortices in near-wall turbulence	June 1997
857	Neishtadt, A. I., D. L. Vainshtein, and A. A. Vasiliev	Chaotic advection in a cubic Stokes flow	June 1997
858	Weaver, R. L.	Ultrasonics in an aluminum foam	July 1997